International Journal of Minerals, Metallurgy and Materials
Volume 26, Number 10, October 2019, Page 1206
https://doi.org/10.1007/s12613-019-1885-7

An analytical solution for evaluating the safety of an exposed face in a paste backfill stope incorporating the arching phenomenon

Xu Zhao[1)], *Andy Fourie*[1)], *and Chong-chong Qi*[2)]

1) School of Civil, Environmental and Mining Engineering, University of Western Australia, Perth 6009, Australia
2) School of Resources and Safety Engineering, Central South University, Changsha 410083, China
(Received: 31 May 2019; revised: 25 June 2019; accepted: 27 June 2019)

Abstract: In current underground mining, the stability of the exposed backfill face is a basic issue associated with mining design and has been the subject of considerable research in mining safety and efficiency. In this study, an improved analytical solution for evaluating the safety of vertically exposed faces in backfilling was proposed. Based on a differential slice method, the proposed solution emphasizes the arching effect as having the advantages of more rigor and wider scalability. Feasibility of the proposed solution was validated with classic centrifuge results. Good agreement between compared results indicated that the proposed solution skillfully predicts the behavior of the paste centrifuge model. Additionally, calculation of exposed face safety in sequential filling was presented. The proposed solution has practical significance in mine backfill design.

Keywords: mine safety; cemented paste backfill; exposed face; arching; sequential filling

1. Introduction

Underground mining has seen an increased use of "cemented paste" for backfilling of stopes [1–5]. In the process of mine backfilling, fill material is deposited back into previously created stopes to improve ground stability and to enhance recovery of ore from pillars [6–8].

When adjacent stopes are extracted, the freestanding surface of fill in the primary stope called "exposed face" will be created, as shown in Fig. 1. Considering the cost of paste backfilling, the backfill design should be cost-effective while capable of ensuring the stability of the exposed face that arises from the strength of the paste. Therefore, in terms of safety and efficiency, accurate prediction of the stability of an exposed backfill face is a crucial issue in backfill design [8].

Although some solutions have been widely applied to predict the strength required of paste in practice, these solutions are generally regarded as conservative in ignoring friction between adjacent rock walls and backfill mass, resulting in unnecessary cost and time delays [9]. Furthermore, most analytical solutions in the literature are still limited in their assumptions of the paste as a uniform material [10]. However, non-uniform distribution of paste strength within the stope may occur due to many factors, such as differing cement contents in each filling stage, especially when the plug pour is applied [10–12], the influence of effective stress development during curing of the paste [13–15], etc. Therefore, a solution incorporating the arching effect that is suitable for both uniform and non-uniform filling paste is needed for mine designs.

In this paper, a new three-dimensional solution applying a differential slice method [16–17] and incorporating arching theory is introduced. It is suitable for the stability evaluation of exposed backfill in mine stopes, including both uniform- and non-uniform-strength paste. After reviewing existing analytical models, the proposed solution and main calculation process are presented. The paper then describes the verification of the proposed solution through comparison of the proposed solution with Mitchell's solution [18] and with classical experimental measurements [9]. Furthermore, the evolution of a cohesive strength of fill in a sequential filling case is represented by a numerical model [19], and

Corresponding author: Chong-chong Qi E-mail: 21948042@student.uwa.edu.au

the evolution of exposed face safety is calculated with the proposed solution. The proposed solution is applicable in sensitivity studies, feasibility studies, and the verification of numerical modeling.

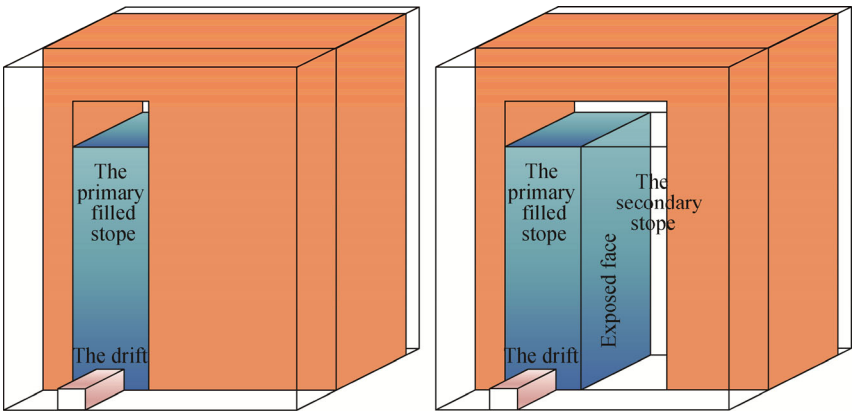

Fig. 1. Schematic showing creation of the vertical exposed face in a typical backfilling scenario.

2. Theoretical analysis

2.1. Traditional self-weight solution

The traditional self-weight solution only considers self-weight stresses during backfill design, which includes requiring the strength of fill to be no less than the maximum of the overburden weight in the stope, given as:

$$[\sigma]_{\mathrm{UCS}} \geq \gamma H \tag{1}$$

where γ is defined as the volume weight of the fill, H is the overall height of the fill, and $[\sigma]_{\mathrm{UCS}}$ is the required uniaxial compressive strength (UCS).

Specifically, for a vertical stope and a uniform strength backfill [18,20]:

$$[\sigma]_{\mathrm{UCS}} \geq \gamma H/2 \tag{2}$$

Ignoring shear effects between the adjacent rock walls and backfill mass, these solutions may result in very conservative design strategies and could be used as upper-bound solutions for a two dimensional plane stope [21]. In order to prevent failure, most backfill in vertical stopes are designed to account for assumed, conservative cohesion of the cement paste backfill (CPB), which means unnecessary cost and time delays for underground mines.

2.2. Mitchell's solution

Currently, Mitchell's solution (MS) is widely used in practice for the safety of the exposed face within a backfilled stope [18]. As a limit equilibrium method, this solution analyzes the mechanical equilibrium of the whole sliding fill mass in the exposed face and considers the mutually supporting effects between backfill and rock walls, as shown in Fig. 2.

According to the confined wedge block model of MS (Fig. 2), the net weight W_{n} of a potential sliding fill mass is:

$$W_{\mathrm{n}} = BH(\gamma L - 2c_{\mathrm{b}}) \tag{3}$$

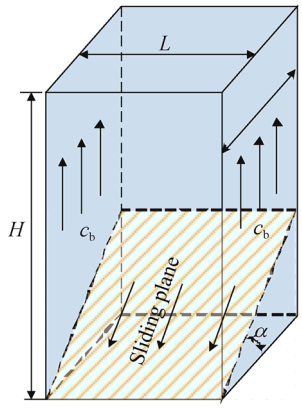

Fig. 2. Confined wedge block model of MS.

The safety factor F is calculated as the resisting forces on the failure plane divided by the driving forces on the failure plane, as follows:

$$F = \frac{W_{\mathrm{n}} \cos\alpha \tan\phi + cLB/\cos\alpha}{W_{\mathrm{n}} \sin\alpha} \tag{4}$$

$$F = \frac{\tan\phi}{\tan\alpha} + \frac{2cL}{H^{*}(\gamma L - 2c_{\mathrm{b}})\sin 2\alpha} \tag{5}$$

where ϕ and c are defined, respectively, as the internal friction angle and apparent cohesion strength of the fill, and α is the angle of the critical plane, taken as 45° + ϕ/2; $H^{*} = H - (B\tan\alpha)/2$ is an equivalent height of the fill mass block; B and L are the width and length of the stope, respectively, and c_{b} is the adhesion strength along the fill and rock wall interface.

Assuming a stope where H is much larger than B and adhesion strength is equal to apparent cohesion of fill ($c_{\mathrm{b}} = c$) and ignoring the friction angle ($\phi = 0$), a simplified expression of the required unconfined compressive strength that

has been easier to use in practice is [18]:

$$[\sigma]_{\mathrm{UCS}} = \frac{\gamma H}{1 + H/L} \tag{6}$$

Generally considered as conservative, this solution is widely used in paste backfilling for underground mining. Over the years, some useful modifications have been proposed based on this solution to adapt to wider geometric boundaries and external mechanical conditions [21–24]. Essentially, these improved solutions are based on the same basic assumption and methodology (equilibrium state of a whole sliding fill mass) as MS.

Despite the advantages of MS and subsequent modifications, some assumptions in these solutions limit a wider application of these methods, including:

(1) Eq. (6) assumes the cemented backfill material as a frictionless material (ϕ = 0) and, therefore, the effect of the frictional shearing resistance to the gravity is ignored [18,20]. According to Mitchell *et al.* [18], the contribution of the ignored frictional shearing resistance to the stability is negligible. However, a 0.33 increase in F can be obtained from the $\tan\phi/\tan\alpha$ part for a typical stope with a ϕ of 33°, which should not be ignored.

(2) Although in MS, adherence effect between fill mass and walls (apparent cohesion c_{b}) has been considered, studies show that there could be more load transfer from the backfill to side walls resulting from shear effect, known as the "arching" phenomenon [25]. Disregarding arching may lead to overestimation of load imposed on the potential sliding surface and therefore a conservative design strategy.

(3) By regarding the sliding wedge as a single, homogenous entity, these solutions assume the shear strength along the sliding face ($\tau = c + \sigma_{\mathrm{n}} \tan\phi$, where σ_{n} is normal stress on the failure plane) to be constant, and therefore, not suitable in the situations when strength of backfill is non-uniform (c and ϕ changing along the sliding surface), as discussed above.

To compensate for the above limitations, an improved analytical solution for estimating the stability of open (unsupported) faces is proposed in this paper.

2.3. Proposed solution

This paper proposes a three-dimensional solution to predict the stability of exposed fill. Proposed solution (PS) is based on Morgenstern's method [16] and the subsequent modified differential slice method [17], which are widely applied in evaluating the stability of soil slopes. For a vertical face of exposed paste backfill, the PS divides the entire potential sliding fill mass into differential vertical slices, as shown in Fig. 3. The vertical stress at the bottom of each slice, considering the arching effect, is then obtained [25–26]. Finally, the PS establishes equations of static equilibrium for each slice and the whole sliding fill mass separately. Here the safety factor F is defined thusly: if the mobilized shear strength of fill along the sliding plane is represented by c/F and $\tan\phi/F$, each element along the sliding plane will simultaneously reach its limiting equilibrium state [17], i.e., $\tau = c_{\mathrm{e}} + \sigma_{\mathrm{n}} \tan\phi_{\mathrm{e}}$, where $c_{\mathrm{e}} = c/F$, $\tan\phi_{\mathrm{e}} = \tan\phi/F$.

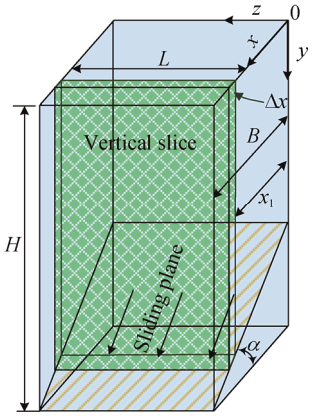

Fig. 3. Differential layer element in wedge block model of PS.

Correct estimation of the stress state within a stope, inter alia, along the potential sliding plane, is essential for safe evaluation of exposed fill face stability. This stress state is mainly influenced by the phenomenon called "arching" that results from the frictional shear stress developed in the wall/fill interfaces [3,27]. Establishing the x and y axes as shown in Fig. 4, a vertical slice at position x_1, with thickness Δx, height H_1, and length L, is taken for analysis. To evaluate the influence of the arching effect on the vertical pressure on the sliding plane, the vertical slice is divided into horizontal layer elements for analysis [25].

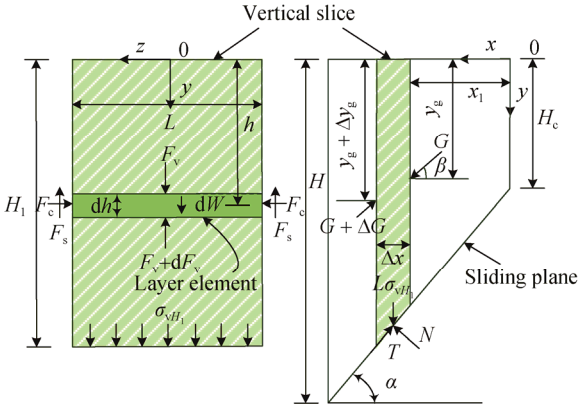

Fig. 4. Horizontal layers and vertical slice with backfill.

As shown in Fig. 4, at position h, the horizontal layer element is subjected to a lateral compressive force F_{c}, a

shearing force F_s, and the vertical forces, F_v; dW represents the weight of this layer of backfill, given by:

$$\mathrm{d}W = \gamma L \mathrm{d}h \tag{7}$$

where dh is the thickness of the layer. Using the relationship between vertical stress σ_v and horizontal stress σ_h in the horizontal element, the lateral compressive force F_c is given by:

$$F_c = \sigma_h \mathrm{d}h = KF_v \mathrm{d}h/L \tag{8}$$

where the reaction coefficient K is the ratio of the lateral stress to the vertical stress:

$$K = \sigma_h / \sigma_v \tag{9}$$

A previous study has indicated that the stress state in backfilled stopes is best described analytically by considering K to be the reaction coefficient of active pressure [1], expressed as:

$$K_a = (1-\sin\phi)(1+\sin\phi) = 0.33 \tag{10}$$

A parametric study of the effect of K is performed in the following section.

The shearing force F_s is defined with the commonly used Coulomb criterion. Considering the surface of rock in the stope is rather rough in practice, the potential vertical sliding surface is likely to be within the paste mass rather than the interface between paste and rock. Hence, the shearing force F_s should include the cohesion of the paste, given as:

$$F_s = (\sigma_h \tan\phi + c)\mathrm{d}h = (KF_v/L\tan\phi + c)\mathrm{d}h \tag{11}$$

By considering the equilibrium of the horizontal layer element, one obtains:

$$F_v + \mathrm{d}F_v + 2F_s = F_v + \mathrm{d}W \tag{12}$$

Introducing Eq. (11) into Eq. (12), the equation is obtained as:

$$\mathrm{d}F_v = \gamma L \mathrm{d}h - 2(KF_v/L\tan\phi + c)\mathrm{d}h \tag{13}$$

By solving Eq. (13), the vertical stress acting across the bottom of the slice σ_{vH_1} can be written as follows:

$$\sigma_{vH_1} = (\gamma L - 2c)\left(\frac{1-\exp(-2KH_1\tan\phi/L)}{2K\tan\phi}\right) \tag{14}$$

The effect of the dimension length L (in Eq. (14)) needs to be noted: when $L \le \dfrac{2c}{\gamma}$, the fill would be self-supporting due to the arching phenomenon; when $L \to \infty$, $\sigma_{vH_1} \to H_1\gamma$, the contribution of the "arching" decreases to zero, turning the case into a plane strain condition. This conclusion agrees with previous research [18].

After obtaining the vertical stress σ_{vH_1}, the force equilibrium and moment equilibrium for each vertical slice need to be reached. As shown in Fig. 4, the term G is the resultant total force acting on the slice, β is the angle between the direction of G and the x direction, and y_g is the point along the y axis at which force G acts.

The static equilibrium of the element in the x and y directions gives:

$$\Delta N\sin\alpha - \Delta T\cos\alpha - \Delta(G\cos\beta) = 0 \tag{15}$$

$$-\Delta N\cos\alpha - \Delta T\sin\alpha + \sigma_{vH_1}L - \Delta(G\sin\beta) = 0 \tag{16}$$

where the parameters T and N are defined as normal force and shear force at the bottom of the vertical fill element, respectively.

Applying Mohr-Coulomb failure criteria and equilibriums of the slice, Eq. (17) is then obtained:

$$\Delta T = c_e \Delta x \sec\alpha + \Delta N\tan\phi_e \tag{17}$$

When $\Delta x \to 0$, substituting Eq. (17) into Eqs. (15) and (16) gives the differential equation of static equilibrium:

$$\cos(\phi-\alpha+\beta)\frac{\mathrm{d}G}{dx} - \sin(\phi-\alpha+\beta)\frac{\mathrm{d}\beta}{dx}G = -p(x) \tag{18}$$

where $p(x)$ is expressed as:

$$p(x) = \frac{\mathrm{d}(L\sigma_{vH_1})}{\mathrm{d}x}\sin(\phi_e-\alpha) - c_e\sec\alpha\cos\phi_e \tag{19}$$

The function $p(x)$ contains the geometrical description of the sliding mass and material parameters of the fill.

Meanwhile, applying the moment equilibrium to the middle point at the bottom of the slice, the following equation is obtained:

$$(G+\Delta G)\cos(\beta+\Delta\beta)\left[(y+\Delta y)-(y_g+\Delta y_g)-\frac{1}{2}\Delta y\right] - G\cos\beta(y-y_g+\frac{1}{2}\Delta y) + G\sin\beta\Delta x = 0 \tag{20}$$

when $\Delta x \to 0$, Eq. (20) is reduced to:

$$G\sin\beta = -y\frac{\mathrm{d}}{\mathrm{d}x}(G\cos\beta) + \frac{\mathrm{d}}{\mathrm{d}x}(y_gG\cos\beta) \tag{21}$$

The boundary conditions of the potential sliding fill mass are:

$$\begin{cases} G(0) = 0 \\ G(B) = 0 \\ y_g(0) = y(0) \\ y_g(B) = \dfrac{2}{3}y(B) \end{cases} \tag{22}$$

Integrating Eq. (21) gives:

$$G(x) = -\sec(\phi_e-\alpha+\beta)s^{-1}(x)\left[\int_0^x p(\zeta)s(\zeta)\mathrm{d}\zeta - G(0)\right] \tag{23}$$

where ζ is the dummy variable, which is used to substitute x in Eq. (23). $s(x)$ is a function expressed as:

$$s(x) = \sec(\phi_e-\alpha+\beta)\exp\left[-\int_0^x \tan(\phi_e-\alpha+\beta)\frac{\mathrm{d}\beta}{\mathrm{d}\zeta}p(\zeta)\right] \tag{24}$$

Eq. (21) can be integrated into:

$$\int_0^x G(\sin\beta - \cos\beta\tan\alpha)\mathrm{d}x = \left[G\cos\beta(y_g-y)\right]_0^x \tag{25}$$

Considering the boundary conditions in Eq. (22), and defining $x = B$, two governing equations are obtained:

$$\int_0^B p(x)s(x)\mathrm{d}x = 0 \tag{26}$$

$$\int_0^B p(x)s(x)t(x)\mathrm{d}x = 0 \tag{27}$$

where

$$t(x) = \int_0^x (\sin\beta - \cos\beta\tan\alpha) \exp\int_0^\xi \left[\tan(\phi_e - \alpha + \beta)\frac{\mathrm{d}\beta}{\mathrm{d}\zeta}\mathrm{d}\zeta\right]\mathrm{d}\xi \tag{28}$$

If Eqs. (26) and (27) are satisfied, the static equilibrium of the potential sliding fill mass can also be achieved. In Eqs. (26) and (27), there are, in total, two unknown variables: safety factor F and angle function $\beta(x)$.

For calculation convenience, it is feasible to assume $\tan\beta = \lambda f(x)$ and $f(x) = 1$, i.e., $\beta(x)$ for each slice is constant [17], so that values of F and the coefficient λ may be found by solving Eqs. (26) and (27).

To get the precise F and λ values that satisfy Eqs. (26) and (27), the Newton-Raphson iteration method was applied.

$$G_n = \int_a^b p(x,F,\lambda)s(x,F,\lambda)\mathrm{d}x \tag{29}$$

$$M_n = \int_a^b p(x,F,\lambda)s(x,F,\lambda)t(x,F,\lambda)\mathrm{d}x \tag{30}$$

where G_n and M_n are the calculated values of force and moment from Eqs. (29) and (30) respectively.

First, the assumed values F_1 and λ_1 were introduced into Eqs. (29) and (30); more accurate values for F_2 and λ_2 can be obtained from the following equations [17]:

$$\Delta F_i = F_{i+1} - F_i = \frac{G_n\frac{\partial M_n}{\partial\lambda} - M_n\frac{\partial G_n}{\partial\lambda}}{\frac{\partial G_n}{\partial\lambda}\frac{\partial M_n}{\partial F} - \frac{\partial G_n}{\partial F}\frac{\partial M_n}{\partial\lambda}} \tag{31}$$

$$\Delta\lambda_i = \lambda_{i+1} - \lambda_i = \frac{-G_n\frac{\partial M_n}{\partial F} + M_n\frac{\partial G_n}{\partial F}}{\frac{\partial G_n}{\partial\lambda}\frac{\partial M_n}{\partial F} - \frac{\partial G_n}{\partial F}\frac{\partial M_n}{\partial\lambda}} \tag{32}$$

The above steps can be repeated until the following convergence criteria are satisfied. In this case, assuming ε = 0.01 has already satisfied the accuracy for engineering:

$$\begin{cases}\Delta F_i < \varepsilon \\ \Delta\lambda_i < \varepsilon\end{cases} \tag{33}$$

It should be noted that tension cracks may develop from the top surface and join the sliding plane in some cases, such as centrifuge tests, presented later in this paper. To ensure the accuracy of the stability analysis, a potential tension crack should be considered [21,26,28–29].

The depth of such a tension crack (H_c) can be estimated by the following expression [29]:

$$H_c = \frac{2c}{\gamma\tan(45^\circ + \phi/2)} \tag{34}$$

In the PS, the influence of tension cracks was embodied in the geometric boundary of the models. Specific calculation considering tension cracks is shown in the following sample calculations.

3. Centrifuge testings validation

To validate the PS, centrifuge testing with detailed information about backfill material properties, instruments, and measurements was chosen for comparison [9]. Safety factors were calculated using the PS, together with critical heights of the prototype fills obtained from centrifuge tests. Critical height (when F = 1) as calculated by the PS was also compared with test results and MS. The objective of these case studies was to determine the accuracy of the PS and to provide calibration for vertical stope backfill faces. Considering the laboratory preparation technique of these models, paste strength was regarded as uniform.

3.1. Centrifuge models

The nominal sizes of the centrifuge models had widths of 200 mm, lengths of 150 mm, and height of 330 mm, controlled by forms fabricated from preserved plywood [9]. Samples were made of 75wt% solids to simulate *in situ* conditions, were cured for 28 d, and were subjected to unconfined compression testing. To simulate a vertical exposed face, a 50 mm spacer was set in the strongbox while pouring slurry into the centrifuge models. The profile of the stope could be seen through the Plexiglas wall of the model. The parameters for these models are listed in Table 1.

Table 1. Unconfined test results of samples

Test No.	Density / ($g\cdot cm^{-3}$)	Water content / wt%	Dry density / ($g\cdot cm^{-3}$)
1	2.03	24.0	1.64
2	1.99	22.7	1.62
3	2.01	23.0	1.63
4	2.06	25.5	1.64
1a	2.09	25.4	1.67
2a	2.07	24.9	1.66
3a	2.06	24.9	1.65
4a	2.08	25.1	1.66

During the centrifuge tests, the speed of the centrifuge was continuously increased until exposed face was damaged,

and acceleration level N was recorded. Table 2 shows the results of these centrifuge tests. Predicted (obtained by Eq. (2)) and experimental prototype heights are also listed. The average ratio of predicted height to that measured was 0.57, indicating that Eq. (2) was highly conservative.

Table 2. Centrifuge test results

Test No.	Unconfined compressive strength / kPa	Prototype height predicted with Eq. (2) / m	Acceleration level at model failure	Experimental prototype height / m
1	96.4	10.9	61.5	20.3
2	96.1	10.9	83.9	27.7
3	101.6	11.5	50.9	16.8
4	101.7	11.5	61.8	20.6
1a	233.0	26.0	158.9	54.5
2a	212.0	22.5	100.0	33.4
3a	418.0	46.6	225.9	74.1
4a	380.0	41.4	214.9	71.8

The failure process was observed as follows: first, a tension crack parallel to the face, at the crest, was observed (approximately 12 cm back from the exposed face). The tension crack then rapidly deepened, followed by the failure of a mass. At the same time, a failure plane appeared near the toe of the model and then extended to join the tension crack. The failure process happened over about 1–5 s. Average strain measured was < 1% when failure occurred, showing the brittle feature of the fill. The photo of failure in model test No.1a is shown in Fig. 5.

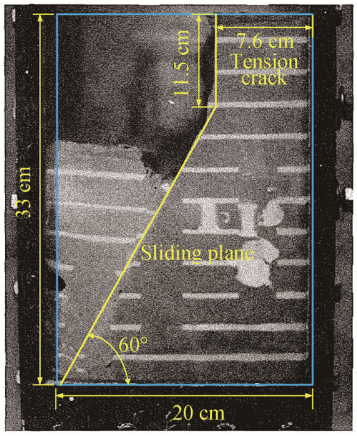

Fig. 5. Failure in model test No. 1a.

3.2. Sample calculation: safety factor of test No. 3 of centrifuge model study

To present an application of the analytical solution proposed in this paper, the same model geometry and backfill properties as used in centrifuge tests were chosen for the analysis. Considering the type of failure mechanism reported in the literature, the geometric parameters for calculation were chosen as: vertical tensile crack occurs at 15 cm (model scale distance) back from the exposed face, and a joint with sliding plane ($\alpha = 60^\circ$) develops from the toe of the backfill. The safety factor calculation process of Test. 3 was as follows:

First, the parameters for the experimental prototype were obtained using conventional centrifuge scaling laws [30] and are shown in Table 3.

Table 3. Parameters used for safety analysis for test No. 3

Height / m	Length / m	Width of failure mass / m	The critical plane angle / (°)	Friction angle / (°)	Length of tensile crack / m	Unit weight / (kN·m^{-3})	UCS strength / kPa
16.8	7.63	7.63	60	30	3.57	17.8	29.3

It should be noted that only unconfined compression tests were conducted on the sample material, which means the apparent cohesion could not be obtained directly. However, the sand was reported to be identical to that used in previous model studies [18], in which the typical ϕ of the sample was about 30°. Other evidence was that a failure plane developing from the toe that was observed during centrifuge tests was at about 60° to the horizontal. In terms of the Coulomb criteria and an active state ($\alpha = 45^\circ + \phi/2$), ϕ was inferred to be 30°. Combining the unconfined strength of 101.6 kPa and ϕ = 30°, the apparent cohesion of the sand used in test No. 3 was calculated as 29.33 kPa by the following equation:

$$c = \frac{\mathrm{UCS}}{2\tan(45^\circ + \phi/2)} \tag{35}$$

Using Eq. (14) to obtain the expression of vertical stress acting across the lower boundary of each slice, then introducing these parameters into the governing Eqs. (29) and (30) and applying the Newton-Raphson method, the results of this iteration are shown in Table 4.

Table 4. Iteration results for test No. 3

Iteration time	F	λ	G_n	M_n	ΔF	$\Delta\lambda$	ε
1	1	1.73	19.95	0	0.09	0	0.01
2	1.09	1.73	0.6	0	0.0008	0	0.01
3	1.09	1.73	—	—	—	—	—

According to the definition of safety factor F, the experimental prototype should reach limiting equilibrium (that is

F = 1) when the centrifuge model fails. The final obtained value of F was 1.09, indicating the PS provided a very good correlation with the results of centrifuge test No. 3. At the same time, convergence of the PS performed very well (with only two calculation steps), reducing computation time and promoting a wider application in mining practice.

3.3. Calculation results analysis and discussion

Safety factors of all eight tests were calculated by both the PS and MS approaches (Eq. (5)), and the results are shown in Fig. 6.

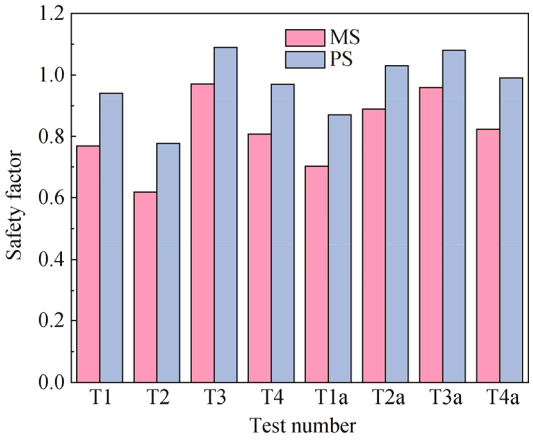

Fig. 6. Safety factors calculated by PS and MS for eight tests.

As shown in Fig. 6, the average predicted safety factor of PS was 0.97. For MS, the error on the calculated safety factor was: $\mathrm{Err}=\sqrt{\sum_{m=1}^{8}(1-F_{\mathrm{MS}}/F_{\mathrm{Measured}})_m^2}=0.61$. When the PS solution was used, the error was: $\mathrm{Err}=\sqrt{\sum_{m=1}^{8}(1-F_{\mathrm{PS}}/F_{\mathrm{Measured}})_m^2}=0.29$. The smaller error of the calculated safety factor indicated that the PS could more accurately predict the experimental results.

3.4. Parametric study of K

For arching theory, three cases were considered for the reaction coefficient K [25]: (1) for pressure at rest, reaction coefficient is: $K=K_0=1-\sin\phi=0.5$; (2) for active pressure, reaction coefficient is expressed as: $K=K_{\mathrm{a}}=(1-\sin\phi)(1+\sin\phi)=0.33$; (3) for passive pressure, reaction coefficient is $K=K_{\mathrm{p}}=(1+\sin\phi)(1-\sin\phi)=3$. The PS calculation results by these three different K values are shown in Fig. 7 for comparison.

As evident from Fig. 7, the safety factor increased when K_{a} was changed to K_0 (average of 1.02) or K_{p} (average of 1.59). This was because an increase in K resulted in more friction between fill and rock wall, thus decreasing the mean stress acting on the sliding plane. In practice, it is generally expected that a large percentage of convergence of the wall may have occurred before backfilling took place, in which case, the K_0 value is preferred.

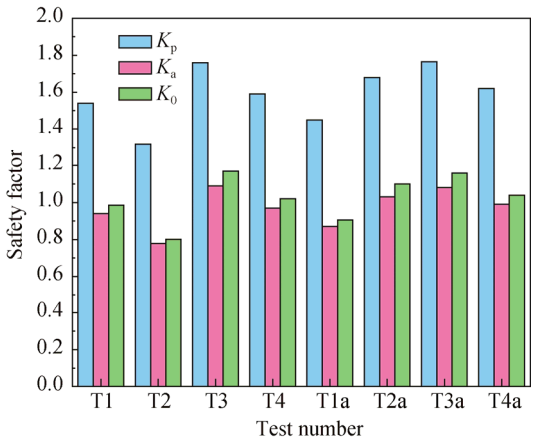

Fig. 7. Safety factors calculated by different K values for eight tests.

When inward convergence of the sidewalls continues after the placement of fill, K_{p} is probably more representative, which would increase the safety factor, according to the PS calculation results. However, the magnitude of this effect could be overestimated because the possible yielding of the fill material due to high mean stress has not been considered in this paper [25].

4. Application of PS in sequential cemented paste fillings

In the pioneering research of exposed face stability, paste was generally assumed to be uniform, which has been called an ideal paste [4,31]. Similarly, most samples prepared in laboratory tests have been regarded as instantaneously poured, and the ultimate strength of cured paste was used for analysis [18,32]. However, strength characteristics of in situ fill within a backfilled stope could be much more complex than this "best case scenario" [31]. First, strength of fill increases with the cement hydration process, i.e., overall safety of the stope is not a fixed factor, but one that evolves with filling process; second, considering a typical filling rate of 5 m/d and a stope 40 m high, it would take eight days to finish the filling operation, when the paste in the bottom of stope may have reached its ultimate cohesion strength, while the surface layer has just been placed, and the hydration process has not even started. Although the paste would finally reach its ultimate strength with the ongoing hydration process, a non-uniform distribution of cohesion strength

could exist until this process finishes in all layers of the paste. Hence, using a uniform and ultimate strength of the fill can lead to an oversimplification of the stability analysis. In other words, if mines can obtain the function between safety factor and curing time, there will be a significant potential contribution to mining efficiency improvement. However, it is not possible to obtain this function unless two problems are solved: (1) whether the analytical solution can solve the non-uniform distribution of strength, and (2) how the strength of cemented paste fill develops with curing time.

As shown in Eqs. (2) and (3), Mitchell's and subsequent solutions are not suitable for prediction purposes when it comes to non-uniform paste backfilling. This is because these earlier solutions apply average shear strength along a sliding plane. An analytical model was developed to study the required strength of an exposed face containing a plug pour [10]. Cohesion of the plug fill was different from that of the final fill, but, being limited by calculation models, they were still constant in respective pours, while friction angle was assumed to be equal across the whole filling.

The new PS can easily accommodate a variation of ϕ and c in the stope when non-uniform characteristics of fill strength are taken into account. Specifically, setting the functions of $\phi(x,y)$ and $c(x,y)$ and introducing them into Eq. (13), the safety factor of an exposed face with non-uniform paste can be obtained. Therefore, the following section focuses on the evolution of cohesive strength versus time and relevant safety analysis in sequential filling cases.

4.1. Distribution and evolution of cohesive strength in sequential fillings

To demonstrate the distribution and evolution of cohesive strength in sequential fillings, cohesion strength distribution in a stope 20 m high, 10 m wide, and 8 m long was modeled by the finite element numerical program "Minefill-2D". Developed for coupled analysis of cementation hydration and stress evolvement in a backfilled stope scenario, Minefill-2D has been verified as capable of providing accurate representation of fill behaviors in mines [15,19]. The model applied a continuous filling strategy with a constant filling rate of 1 m/d and assumed a constant frictional angle. Filling strategy and properties describing the cement behavior are listed in Table 5.

In Minefill-2D, a function is applied to describe the cumulative development of cement cohesion, shown as:

$$\frac{\partial c}{\partial t}=\frac{1}{2}\left(\frac{d}{(t-t_0)^{1.5}}\right)\exp\left(\frac{-d}{\sqrt{t-t_0}}\right)A\exp\left(\frac{XC_c+C_c^{0.1}-e}{ZC_c}\right) \quad (36)$$

Eq. (36) includes those parameters describing the maturity and efficiency of the hydration process, where t is the time after placement, t_0 is the initial set of hydration processes, d is the rate of the hydration parameter, C_c is the cement content (weight of cement per unit weight of solids), e is void ratio, A, X, and Z are curve fitting constants.

Material of the fill was paste fill A (PFA); all of these parameters were obtained experimentally, and the derivation process of Eq. (36) was introduced with details [4].

Fig. 8 shows the contours of cohesion strength within the backfilled stope at different times. At the end of filling, the

Table 5. Properties of materials used across cases

Wet unit weight / ($kN·m^{-3}$)	Rate of hydration parameter / ($d^{1/2}$)	Initial set / d	Constant A / ($cm^3·g^{-1}$)	Cement content / wt%	Friction angle / (°)	Filling rate / ($m·d^{-1}$)	Constant X	Constant Z
18.1	1.4	0.3	0.032	1.5	30	5	1.8	–0.2

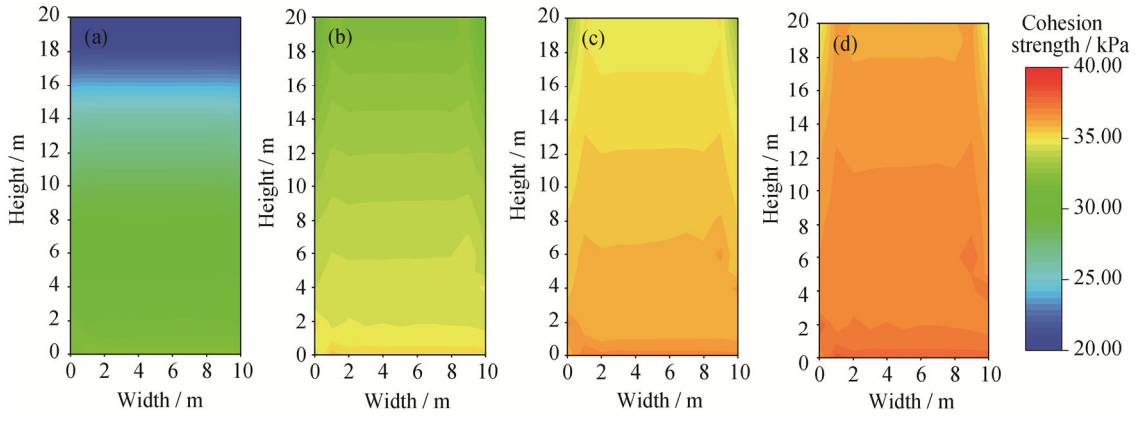

Fig. 8. Distribution of cohesion strength at (a) end of filling, (b) 4 d after filling, (c) 8 d after filling, and (d) 12 d after filling.

paste within the stope showed a remarkable layered distribution of strength, with 32.2 kPa at the bottom and 20 kPa at the surface. With ongoing curing, the fill from the bottom to top continually increased and gradually reached the ultimate strength of 37.8 kPa at 12 d after the filling.

4.2. Development of model safety factor

Combining the non-uniform distribution of cohesion strength obtained by finite element software Minefill-2D, the function of the safety factor changing with time could be obtained by the PS. To further demonstrate the PS, the calculation process of safety factor with non-uniform strength at the end of filling is given as follows: fitting the cohesion strength along the potential sliding plane ($\alpha = 60^\circ$) with x axis direction ($0 \le x \le 10$) into a function, $c(x) = -0.1068x^2 - 6E - 5x + 31.32$. Results of each iterations are listed in Table 6.

Table 6. Iteration results of safety factor at the end of filling

Iteration time	F	λ	G_n	M_n	ΔF	$\Delta\lambda$	ε
1	1	1.73	–275.4	0	–0.281	0	0.01
2	0.718	1.73	108.0	0	0.057	0	0.01
3	0.775	1.73	7.95	0	0.004	0	0.01
4	0.779	1.73	—	—	—	—	—

After three iteration steps, the final safety factor F converged to 0.779, indicating it was dangerous if the exposed face was created at the end of filling. Similarly, safety factors at different times were calculated, and the curve of safety factor versus time are shown in Fig. 9.

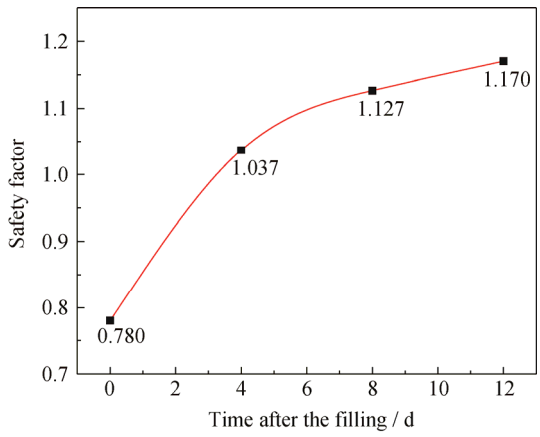

Fig. 9. Effect of time on calculated safety factor.

As shown in Fig. 9, the curve began at 0.78 at the end of filling and continually increased with the ongoing hydration process. Calculated safety factor reached 1 at about 3.5 d and then tended toward 1.17 after 12 d.

The above section presents the calculation procedure of exposed face safety accounting for the non-uniform distribution and evolution of cohesion strength versus curing time, which paves the way for potential application in the safety design of the backfilled stope.

5. Discussion

To evaluate stability of the exposed face in the backfilled stope, an improved three-dimensional analytical solution that considers the frictional resistance between the backfill and stope walls (i.e., accounting for the arching effect) is proposed. The derivation was based on Morgenstern's original method [16] as well as subsequent modifications [17] that were developed for analysis of slope stability problems.

To verify application of the PS, the classic MS [18] and centrifuge tests [9] were chosen for comparison. Results showed that, for a given cohesion and angle of internal shear, PS provides a good prediction of the experimentally measured failure heights (and thus the factor of safety). Furthermore, when compared with the MS, the predicted failure height with PS is more accurate in experimental testings.

Although the PS favorably represents the experimental results, it has some limitations. For instance, the cohesion c of the paste varies linearly (changing with elevation) in the numerical model of sequential filling. However, some *in situ* measurements and physical simulation experiments [31] have shown the actual strength distribution may be more complex. Various mechanisms such as segregation upon deposition and imposed effective stress during curing have both influenced the ultimate strength of the fill [13]. In future research, some regular qualitative distributions of paste strength could be considered in more detail. In practice, mines using backfill could obtain in situ strengths of the CPB using suitable techniques, such as coring followed by tri-axial testing. Setting functions $\phi(x, y)$ and $c(x, y)$ to represent these characteristics, the PS could provide more precise case-based predictions.

A key assumption in this paper is the shape of the sliding surface. The assumption of a flat sliding surface was proposed and proved to be effective in mine backfill design [18]. However, it should be noted that this assumption is somewhat a simplification. According to a series of laboratory experimental results, the profile of the sliding surface is actually a slightly curved surface [18], while the whole sliding surface is more concave than flat [33]. This trend becomes even clearer in models with a high ratio of height to length (H/L). This phenomenon probably results from the mutually supporting effects of fill and walls, causing some of the fill

mass to adhere to the wall. Exploration of this mechanism and improvement of the PS for concave sliding surface is ongoing.

In addition to providing accurate predictions for a uniform strength paste model, this paper also evaluated the condition where *in situ* strength distribution characteristics may be more complex than uniform, thus taking into account factors such as curing time and maturity of the hydration process in cemented paste backfill. While most current methods are unable to deal with such non-uniformities, the PS is suitable for calculating the stability of a paste-filled stope having a non-uniform strength distribution, taking advantage of the differential slice method.

6. Conclusions

An improved three-dimensional analytical solution considering arching effects is proposed in this paper. The proposed analytical solution provides a useful stability calculation model. Compared to previous analytical solutions for evaluating the exposure stability of ideal (i.e., uniform strength) paste fill, the PS has wider applicability (both uniform and non-uniform strength) and accuracy, as verified by the centrifuge test data presented and discussed. If combined with an investigation of particular field situations (e.g., *in situ* strength characteristics of the paste), the safety factor of the stope (for given backfilling dimensions and paste fill properties) or the allowable backfilling height (for a given strength of paste) can be obtained using the PS. Therefore, the PS can be used by paste backfill design engineers as a more rational approach to predicting exposed face safety and for specification of required strength properties.

Acknowledgement

This work was financially supported by the China Scholarship Council (No. 201506420049).

References

[1] L. Li and M. Aubertin, Horizontal pressure on barricades for backfilled stopes. Part I: Fully drained conditions, *Can. Geotech. J.*, 46(2009), No. 1, p. 37.

[2] C.C. Qi and A. Fourie, Cemented paste backfill for mineral tailings management: Review and future perspectives, *Miner. Eng.*, 144 (2019), art. No. 106025.

[3] M. Fahey, M. Helinski, and A. Fourie, Some aspects of the mechanics of arching in backfilled stopes, *Can. Geotech. J.*, 46(2009), No. 11, p. 1322.

[4] M. Helinski, M. Fahey, and A. Fourie, Behavior of cemented paste backfill in two mine stopes: measurements and modeling, *J. Geotech. Geoenviron. Eng.*, 137(2010), No. 2, p. 171.

[5] C. Hou, W.C. Zhu, B.X. Yan, K. Guan, and J.F. Du, Influence of binder content on temperature and internal strain evolution of early age cemented tailings backfill, *Constr. Build. Mater.*, 189(2018), p. 585.

[6] N. Zhou, J.X. Zhang, H. Yan, and M. Li, Deformation behavior of hard roofs in solid backfill coal mining using physical models, *Energies*, 10(2017), No. 4, p. 557.

[7] N. Zhou, X. Han, J. Zhang, and M. Li, Compressive deformation and energy dissipation of crushed coal gangue, *Powder Technol.*, 297(2016), p. 220.

[8] T. Belem and M. Benzaazoua, Design and application of underground mine paste backfill technology, *Geotech. Geol. Eng.*, 26(2008), No. 2, p. 147.

[9] R.J. Mitchell, Centrifuge model tests on backfill stability, *Can. Geotech. J.*, 23(1986), No. 3, p. 341.

[10] L. Li, Analytical solution for determining the required strength of a side-exposed mine backfill containing a plug, *Can. Geotech. J.*, 51(2014), No. 5, p. 508.

[11] B.D. Thompson, M.W. Grabinsky, W.F. Bawden, and D.B. Counter, *In-situ* measurements of cemented paste backfill in long-hole stopes, [in] *ROCKENG09: Proceedings of the 3rd CANUS Rock Mechanics Symposium*, Toronto, 2009, p. 199.

[12] B.D. Thompson, W.F. Bawden, and M.W. Grabinsky, *In situ* measurements of cemented paste backfill at the Cayeli Mine, *Can. Geotech. J.*, 49(2012), No. 7, p. 755.

[13] M. Fahey, M. Helinski, and A. Fourie, Development of specimen curing procedures that account for the influence of effective stress during curing on the strength of cemented mine backfill, *Geotech. Geol. Eng.*, 29(2011), No. 5, p. 709.

[14] A. Fourie, M. Helinski, and M. Fahey, Using effective stress theory to characterize the behaviour of backfill, *CIM MAG.*, 100(2007), No. 1103, p. 27.

[15] M. Helinski, M. Fahey, and A. Fourie, Coupled two-dimensional finite element modelling of mine backfilling with cemented tailings, *Can. Geotech. J.*, 47(2010), No. 11, p. 1187.

[16] N.R. Morgenstern and V.E. Price, A numerical method for solving the equations of stability of general slip surfaces, *Comput. J.*, 9(1967), No. 4, p. 388.

[17] Z.Y. Chen and N.R. Morgenstern, Extensions to the generalized method of slices for stability analysis, *Can. Geotech. J.*, 20(1983), No. 1, p. 104.

[18] R.J. Mitchell, R.S. Olsen, and J.D. Smith, Model studies on cemented tailings used in mine backfill, *Can. Geotech. J.*, 19(1982), No. 1, p. 14.

[19] M. Helinski, *Mechanics of Mine Backfill* [Dissertation], University of Western Australia, Perth, 2007.

[20] L. Li and M. Aubertin, An improved analytical solution to estimate the stress state in subvertical backfilled stopes, *Can. Geotech. J.*, 45(2008), No. 10, p. 1487.

[21] L. Li and M. Aubertin, A modified solution to assess the required strength of exposed backfill in mine stopes, *Can.*

Geotech. J., 49(2012), No. 8, p. 994.

[22] S. Zou and N. Nadarajah, Optimizing backfill design for ground support and cost saving, [in] *Golden Rocks 2006, The 41st US Symposium on Rock Mechanics (USRMS)*, Golden, 2006.

[23] A.P.E. Dirige, R.L. McNearny, and D.S. Thompson, The effect of stope inclination and wall rock roughness on back-fill free face stability, [in] *Rock Engineering in Difficult Conditions: Proceedings of the 3rd Canada–US Rock Mechanics Symposium*, Toronto, 2009.

[24] A.P.E. Dirige and E. De Souza, Engineering design of backfill systems in adjacent pillar mining, [in] *The 42nd US Rock Mechanics Symposium (USRMS)*, San Francisco, 2008.

[25] M. Aubertin, L.S.T.B.M. Li, S. Arnoldi, T. Belem, B. Bussière, M. Benzaazoua, and R. Simon, Interaction between backfill and rock mass in narrow stopes, *Soil rock Am.*, 1(2003), p. 1157.

[26] D.F. McCarthy, *Essentials of Soil Mechanics and Foundations*, Reston Publishing Company, Reston, 1977, p. 505.

[27] B. Yan, W. Zhu, C. Hou, and K. Guan, A three-dimensional analytical solution to the arching effect in inclined backfilled stopes, *Geomech. Geoeng.*, 14(2019), No. 2, p. 136.

[28] J.D. Smith, C.L. Dejongh, and R.J. Mitchell, Large scale model tests to determine backfill strength requirements for pillar recovery at the Black Mountain Mine, [in] *Proceedings of International Symposium on Mining With Backfill*, Lulea, 1983, p. 7.

[29] K. Terzaghi, *Theoretical Soil Mechanics*, Limited John Wiler And Sons. Inc, New York, 1944.

[30] A.N. Schofield, Use of centrifugal model testing to assess slope stability, *Can. Geotech. J.*, 15(1978), No. 1, p. 14.

[31] Q.S. Chen, Q.L. Zhang, A. Fourie, X. Chen, and C.C. Qi, Experimental investigation on the strength characteristics of cement paste backfill in a similar stope model and its mechanism, *Constr. Build. Mater.*, 154(2017), p. 34.

[32] R.J. Mitchell, Model studies on the stability of confined fills, *Can. Geotech. J.*, 26(1989), No. 2, p. 210.

[33] X.W. Yi, G.W. Ma, and A. Fourie, Centrifuge model studies on the stability of fibre-reinforced cemented paste backfill stopes, *Geotext. Geomembr.*, 46(2018), No. 4, p. 396.